

Unstable quasiparticles as a source of thermodynamic instabilities in the thermal nonlocal Nambu-Jona-Lasinio model.

F. Marquez

Facultad de Física, Pontificia Universidad Católica de Chile, Casilla 306, Santiago 22, Chile.

It has already been shown that in thermal nonlocal Nambu-Jona-Lasinio models some unphysical behavior, such as a negative pressure, may arise. In this article, it is argued that such behavior is a consequence of considering bound states of highly unstable quasiparticles and tachyons that are present in the model. Computations are carried out within the real time formalism which allows to isolate the contributions from different quasiparticles and identify the source of these instabilities. It has also been shown how these instabilities are softened by the inclusion of the Polyakov loop. This article shows how this softened instabilities may be understood by studying the effect of the Polyakov loop on the quasiparticles of the model.

I. INTRODUCTION

There are several aspects of QCD, like the mechanism behind quark confinement or the phase diagram, that are not yet fully understood. Several models have been developed in order to describe some of these properties, such as the bag model [1–4], Dyson-Schwinger models [5–7] and the linear sigma model [8–11]. Another attempt in this direction is the Nambu-Jona-Lasinio (NJL) model [12, 13]. Although it was originally proposed as a model of interacting nucleons, the NJL model is now interpreted as model of interacting quarks and is vastly used to study thermal properties of QCD [14–18].

The nonlocal Nambu-Jona-Lasinio (nNJL) model is a generalization of the NJL model [19, 20] with a nonlocal interaction that is modulated by a regulator. The nNJL model is also used to study thermal properties of QCD [21–25]. Thermal computations in nNJL models are usually carried out using the imaginary time formalism. Although calculations are usually simpler in the imaginary time formalism, the physical interpretation of the propagator can be a bit cumbersome. However, in the real time formalism the quark propagator has the usual structure where we have singularities that can be interpreted as quasiparticles. This structure of the propagator allows us to manipulate expressions in order to study all, or only a few of the quasiparticles contributions. Expressions in the real time formalism will usually have the form of a zero temperature contribution plus several terms from thermal contributions, each of them corresponding to a different pole of the propagator. This allows us to track different poles by isolating their contributions to some thermal quantity like the chiral condensate.

In a few recent articles it has been shown that some unphysical instabilities arise within these models [26, 27] which, however, are softened by the inclusion of the Polyakov loop. This article shows that these instabilities arise because one is considering highly unstable poles of the propagator and tachyons. The physical input from the quasiparticle interpretation for the poles of the

propagator, allows to comment on the reasons behind these instabilities and their relation with unstable poles. In this manner it is possible to isolate the contributions of different quasiparticles and study their relation to the appearance of thermal instabilities. The Polyakov loop is then included in the model. By doing so, one is also incorporating new singularities into the propagator. Then, the behavior of these new singularities can be studied in order to see if there is any reason for the Polyakov loop to soften the thermal instabilities present in the model. In this article, it is shown how these new poles included through the Polyakov loop are less unstable poles and, hence, one would expect for them to soften the thermal instabilities. The most commonly used regulators: the Gaussian and the Lorentzian regulators, are considered in this article. Thermal instabilities are present and they can be related to the presence of unstable poles. These thermal instabilities can be removed in some cases by a careful selection of poles or by a different choice in the parameters of the model.

The paper is organized as follows. In Sec. II, the nNJL model is introduced and the real time formalism is developed in a general manner. In Sec. III the formalism is applied to the Gaussian regulator. In Sec. IV the formalism is applied to an integer Lorentzian regulator and in Sec. V to a fractional Lorentzian regulator. In Sec. VI a few remarks on how these instabilities may be handled are made. In Sec. VII a brief discussion on the inclusion of the Polyakov loop in the model and how this affects the quasiparticles behavior and the occurrence of thermal instabilities is presented. In Sec. VIII conclusions are presented.

II. nNJL MODEL IN REAL TIME FORMALISM.

The nNJL model is described through the Euclidean Lagrangian

$$\mathcal{L}_E = \left[\bar{\psi}(x)(-i\not{D} + m)\psi(x) - \frac{G}{2}j_a(x)j_a(x) \right], \quad (1)$$

with $\psi(x)$ being a quark field. The nonlocal aspects of the model are incorporated through the nonlocal currents $j_a(x)$

$$j_a(x) = \int d^4y d^4z r(y-x)r(z-x)\bar{\psi}(x)\Gamma_a\psi(z), \quad (2)$$

where $\Gamma_a = (1, i\gamma^5\vec{\tau})$. A bosonization procedure can be performed by defining scalar (σ) and pseudoscalar ($\vec{\pi}$) fields. Then, in the mean field approximation,

$$\sigma = \bar{\sigma} + \delta\sigma \quad (3)$$

$$\vec{\pi} = \delta\vec{\pi}, \quad (4)$$

where $\bar{\sigma}$ is the vacuum expectation value of the scalar field, i.e. $\bar{\sigma} = G\langle\bar{\psi}\psi\rangle$. In this manner, $\bar{\sigma}$ is closely related to the quiral condensate, and they must behave in exactly the same manner. Also, it was assumed for the pseudoscalar field to have a null vacuum expectation value because of isospin symmetry. Quark fields can then be integrated out of the model [23, 28] and the mean field effective action can be obtained

$$\Gamma^{MF} = V_4 \left[\frac{\bar{\sigma}^2}{2G} - 2N_c \int \frac{d^4q_E}{(2\pi)^4} \text{tr} \ln S_E^{-1}(q_E) \right], \quad (5)$$

with $S_E(q_E)$ being the Euclidean effective propagator

$$S_E = \frac{-\not{q}_E + \Sigma(q_E^2)}{q_E^2 + \Sigma^2(q_E^2)}. \quad (6)$$

Here, $\Sigma(q_E^2)$ is the constituent quark mass

$$\Sigma(q_E^2) = m + \bar{\sigma}r^2(q_E^2). \quad (7)$$

Finite temperature (T) effects can be incorporated through the Matsubara formalism. To do so, one can make the following substitutions

$$V_4 \rightarrow V/T \quad (8)$$

$$q_4 \rightarrow -q_n \quad (9)$$

$$\int \frac{dq_4}{2\pi} \rightarrow T \sum_n, \quad (10)$$

where q_n includes the Matsubara frequencies

$$q_n \equiv (2n+1)\pi T. \quad (11)$$

With this, the propagator in Eq. (6) will now look like

$$S_E(q_n, \mathbf{q}, T) = \frac{\gamma^4 q_n - \gamma \cdot \mathbf{q} + \Sigma(q_n, \mathbf{q})}{q_n^2 + \mathbf{q}^2 + \Sigma^2(q_n, \mathbf{q})}. \quad (12)$$

It is worth noting that the propagator in Eq. (12) has no singularities. Since there are no poles at some p^2 , the definition of an effective mass for the particle with such propagator is non trivial. Because of this it is harder to physically understand and interpret some quantities in the imaginary time formalism.

The σ field will evolve with temperature. This evolution can be computed through the grand canonical thermodynamical potential in the mean field approximation $\Omega_{MF}(\bar{\sigma}, T, \mu) = (T/V)\Gamma_{MF}(\bar{\sigma}, T, \mu)$ [29]. Then the value of $\bar{\sigma}$ must be at the minimum of the potential where $\partial\Omega_{MF}/\partial\bar{\sigma} = 0$, which means

$$\frac{\bar{\sigma}}{G} = 2N_c T \sum_n \int \frac{d^3q}{(2\pi)^3} r^2(q_E^2) \text{tr} S_E(q_E) \Big|_{q_4=-q_n}. \quad (13)$$

From this equation one can get the temperature evolution of $\bar{\sigma}$. The next step is to workout the model in the real time formalism. In order to do so one should first perform a Wick rotation $q_4 = iq_0$ that will take us from Euclidean to Minkowski space. Doing this in Eq. (6) will yield the zero temperature Minkowski space propagator

$$S_0 = i \frac{\not{q} + \Sigma(-q^2)}{q^2 - \Sigma^2(-q^2)}, \quad (14)$$

where $q^2 = -q_E^2$. This propagator has singularities in the complex q^2 plane. Each of these singularities may be interpreted as a different quasiparticle of the model. Then, it is possible to define a mass and a decay width for the quasiparticles. If $q^2 = \mathcal{M}^2$ is a singularity of the propagator, the following definition can be made

$$q^2 = \mathcal{M}^2 = M^2 + iM\Gamma, \quad (15)$$

where M is the constituent mass of the quasiparticle and Γ its decay width. The next step is to obtain the thermal propagator in the real time formalism.

In the real time formalism, the number of degrees of freedom is doubled [30–35]. This means that the thermal propagator is given by a 2×2 matrix with elements S_{ij} . However, in one-loop calculations only the S_{11} component is necessary. A general expression for S_{11} can be written in terms of the spectral density function (SDF)

$$S_{11} = \int \frac{dk_0}{2\pi i} \frac{\rho(k_0, \mathbf{q})}{k_0 - q_0 - i\varepsilon} - n_F(q_0)\rho(q), \quad (16)$$

where $n_F(q_0)$ is the Fermi-Dirac distribution $n_F(q_0) = (e^{q_0/T} + 1)^{-1}$. The SDF can be obtained from

$$\rho(q) = S_+(q) - S_-(q), \quad (17)$$

where

$$S_{\pm}(q) = \pm \oint_{\Gamma_{\pm}} \frac{dz}{2\pi i} \frac{S_0(z \mp i\varepsilon, \mathbf{q})}{z - q_0 \pm i\varepsilon}. \quad (18)$$

This is just a generalization of the free particle case where $\rho(q) = S_0(q_0 + i\varepsilon, \mathbf{q}) - S_0(q_0 - i\varepsilon, \mathbf{q})$. The integration path Γ^{\pm} is shown in Fig. 1.

The integrations can be performed and the SDF can be found to be

$$\rho(q) = \sum_{\mathcal{M}} i \left[\frac{A(\mathcal{M}^2)}{\mathcal{M}^2 - q^2} - \frac{A((\mathcal{M}^2)^*)}{(\mathcal{M}^2)^* - q^2} \right] \quad (19)$$

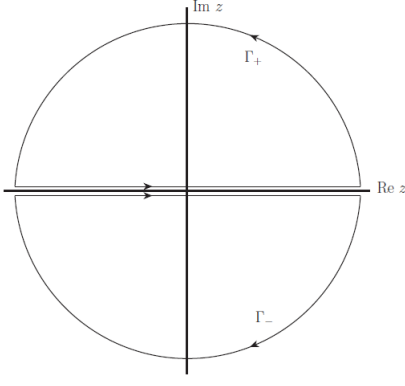


FIG. 1. Integration path in the definition of S_{\pm} .

where the sum is over the various poles (\mathcal{M}) of the propagator and

$$A(\mathcal{M}^2) = \frac{Z(\mathcal{M}^2)}{2E} (q_0(\not{q} + \Sigma(-\mathcal{M}^2)) - \gamma^0(q^2 - \mathcal{M}^2)), \quad (20)$$

with $E^2 = \mathcal{M}^2 + q^2$ and where

$$Z(\mathcal{M}^2) = \left[\frac{\partial}{\partial q^2} (q^2 - \Sigma^2(-q^2)) \right]^{-1} \Big|_{q^2 = \mathcal{M}^2}, \quad (21)$$

is the renormalization constant. It is worth noting that in Eq. (19) the contributions from each pole to the SDF are decoupled from each other. This structure is crucial since it allows to isolate the contribution from each pole. The real time thermal propagator can then be obtained by putting Eq. (19) into Eq. (16). It is clear that the propagator will also have the same structure of the SDF in the sense that contributions from different poles are decoupled from each other. Moreover the propagator will also have the zero temperature contribution decoupled from the finite temperature one, i.e.

$$S_{11}(q, T, \mu) = S_0(q) + \tilde{S}(q, T). \quad (22)$$

Of course, in the case where $\Gamma \rightarrow 0$, i.e. when considering real poles, then the propagator reduces to the usual Dolan-Jackiw propagator [36]

$$S_{DJ}(q, M) = (\not{q} + M) \left[\frac{i}{q^2 - M^2 + i\varepsilon} - 2\pi N(q_0) \delta(q^2 - M^2) \right] \quad (23)$$

The gap equation in the real time formalism should now be obtained through the substitution $S_E \rightarrow S_{11}$ in Eq. (13). Using the structure in Eq. (22) yields

$$\frac{\partial \Omega_{MF}}{\partial \bar{\sigma}} = g_0(\bar{\sigma}) + \tilde{g}(\bar{\sigma}, T) = 0, \quad (24)$$

where

$$g_0(\bar{\sigma}) = \frac{\bar{\sigma}}{G} - \frac{N_c}{\pi^2} \int_0^\infty dq_E q_E^3 \frac{r^2(q_E^2) \Sigma(q_E^2)}{q_E^2 + \Sigma^2(q_E^2)} \quad (25)$$

$$\tilde{g}(\bar{\sigma}, T) = -2N_c \int \frac{d^4 q}{(2\pi)^4} r^2(-q^2) \text{tr} \tilde{S}(q, T), \quad (26)$$

and where again $\tilde{g}(\bar{\sigma}, T)$ has all of the finite temperature contribution. By putting the expression for \tilde{S} into Eq. (26) we get

$$\begin{aligned} \tilde{g}(\bar{\sigma}, T) &= 2iN_c \sum_{\mathcal{M}} Z(\mathcal{M}^2) \Sigma(-\mathcal{M}^2) \\ &\times \int \frac{d^4 q}{(2\pi)^4} \frac{r^2(-q^2)}{E} 2n_F(q_0) \\ &\times \left[\frac{q_0}{\mathcal{M}^2 - q^2} - \frac{q_0}{(\mathcal{M}^2)^* - q^2} \right] + C. \end{aligned} \quad (27)$$

The integration in q_0 can be performed along the path shown in Fig. 2.

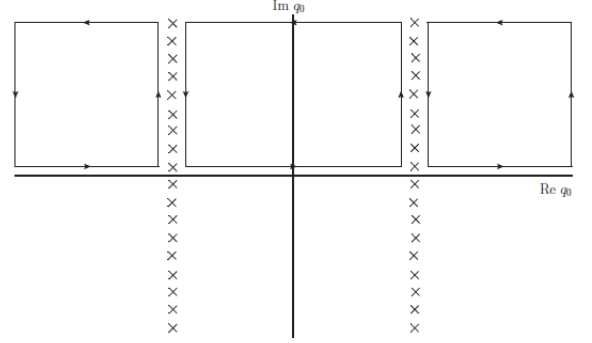


FIG. 2. Integration path for the thermal part of the gap equation. The poles of the Fermi-Dirac distribution are marked with crosses

The integration along the vertical lines where $\text{Re } q_0 \rightarrow \pm\infty$ gives a divergent contribution that, however, is independent of temperature and will be cancelled by the constant C in Eq. (27). The integration then can be computed to give

$$\begin{aligned} \tilde{g}(\bar{\sigma}, T) &= -\frac{N_c}{\pi^2} \sum_{\mathcal{M}} [Z(\mathcal{M}^2) \Sigma(-\mathcal{M}^2) r^2(-\mathcal{M}^2) \\ &\times \int dk k^2 \frac{2n_F(E)}{E} + (\mathcal{M}^2 \rightarrow (\mathcal{M}^2)^*)]. \end{aligned} \quad (28)$$

This is the final expression for the gap equation in the real time formalism. Once again, this expression has the contributions from different poles decoupled from each other. This will allow to isolate the contributions of each pole. Every quasiparticle mass and decay width will evolve with temperature. If we are interested in studying the behaviour of just one quasiparticle by itself, we can toss all of the other terms in Eq. (28) coming

from different poles and solve solely for the quasiparticle we are interested in. Formally, this can be done by deforming the integration path in Fig. 1 around the undesired poles in order to exclude them. This will be of the most importance when trying to identify the source of the unphysical thermal instabilities that arise in this type of models.

The main quantity we are going to look at is $\bar{\sigma}$. It should behave in the same manner as a chiral condensate. This means that one would expect for $\bar{\sigma}$ to monotonically decrease as temperature increases. Otherwise, we would have a condensate that becomes larger at larger temperatures. The gap equation in Eq. (28) will allow us to get the behavior of $\bar{\sigma}$ as a function of temperature. Any growth of $\bar{\sigma}$ will then be considered an “instability” since it does not correspond to the usual behavior of a condensate. However, it will be shown that these instabilities may be understood through the quasiparticle interpretation of the poles of the propagator.

III. GAUSSIAN REGULATOR.

Let us now consider the nNJL model with a Gaussian regulator of the form

$$r(q^2) = e^{q^2/\Lambda^2}. \quad (29)$$

Two different sets of parameters will be considered for this regulator. They are conveniently chosen because of the pole structure the propagator exhibits with such parameters. The parameters are shown in Table I. Set A is taken from reference [26] and set B from [37].

Set	$\Lambda(\text{MeV})$	$m(\text{MeV})$	$G\Lambda^2$	$\bar{\sigma}_0(\text{MeV})$
A	687	6	28.43	677.8
B	1042.2	4.6	15.08	235

TABLE I. Both parameters set used for the Gaussian regulator case. $\bar{\sigma}_0$ is the mean value of the scalar field at zero temperature.

Then, by solving $q^2 - \Sigma^2(-q^2) = 0$ one can find the poles of the propagator, which means

$$\text{Re}(q^2 - \Sigma^2(-q^2)) = 0 \quad (30)$$

$$\text{Im}(q^2 - \Sigma^2(-q^2)) = 0. \quad (31)$$

Fig. 3 shows the solutions to Eqs. (30) and (31). The poles of the propagator are found in the intersections of the dashed and solid lines. There is one important thing to note here. For set of parameters A (left plot in Fig. 3) the first pole has a negative real part. Since these are poles in the q^2 complex plane, then a negative real part corresponds to a negative squared mass, i.e. particles with imaginary masses or tachyons [38–40]. One should expect some kind of odd behavior from such

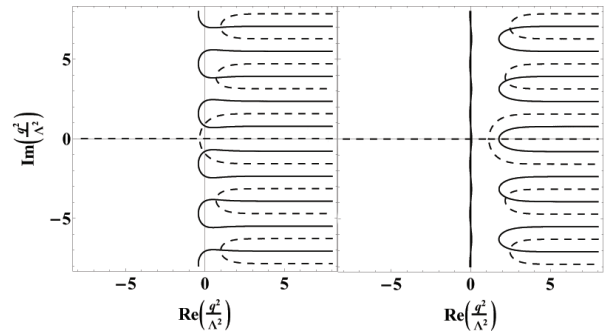


FIG. 3. Poles of the propagator for the Gaussian regulator in the q^2 plane. The left plot is for set A and the right plot for set B. The dashed lines are solutions to Eq. (31) and the solid lines solutions to Eq. (30).

a quasiparticle and, in fact, it will be argued that these poles are mainly responsible for the thermal instabilities that will be found later. For parameter set B however (right plot in Fig. 3) there is no such pole. Instead, we have that the first two poles are real and positive. In both cases we have an infinite number of poles. In what follows we will only consider some of them. This will suffice to show the presence of instabilities and how they relate to the poles of the propagator.

Our next step is to solve Eq. (28) in order to get the behavior of $\bar{\sigma}$ as a function of temperature. As was mentioned, $\bar{\sigma}$ is closely related to the chiral condensate and it should behave in the same manner. However, it may be the case that negative squared mass quasiparticles are present in our propagator. It is reasonable to expect some odd behavior of $\bar{\sigma}$ in the presence of such a quasiparticle. On the other hand, a pole with positive real part and vanishing imaginary part is a stable particle and one would expect from it the usual behavior of a condensate. This makes the study of the poles of the propagator a crucial matter in order to understand the behavior of $\bar{\sigma}$. Because of this, before solving Eq. (28), it is important to take a closer look to the poles of the propagator.

Fig. 4 shows the behavior of the first three poles of the propagator for both sets as a function of $\bar{\sigma}$. As can be seen, the first pole of set A has a negative real part for $\bar{\sigma} = \bar{\sigma}_0$. However, at lower values, $\bar{\sigma} \approx 300$ MeV, the pole has a positive real part and a vanishing imaginary part, i.e. it has turned into a positive real pole. On the other hand, for set B, we have two positive real poles and no pole with a negative real part. All of the other poles will turn out to be poles with positive real parts and nonvanishing imaginary parts. They will, however, be more massive than the poles here considered and should have smaller contributions to the behavior of $\bar{\sigma}$. Let us

now solve Eq. (28) for these three poles in order to get $\bar{\sigma}$ as a function of temperature for both sets.

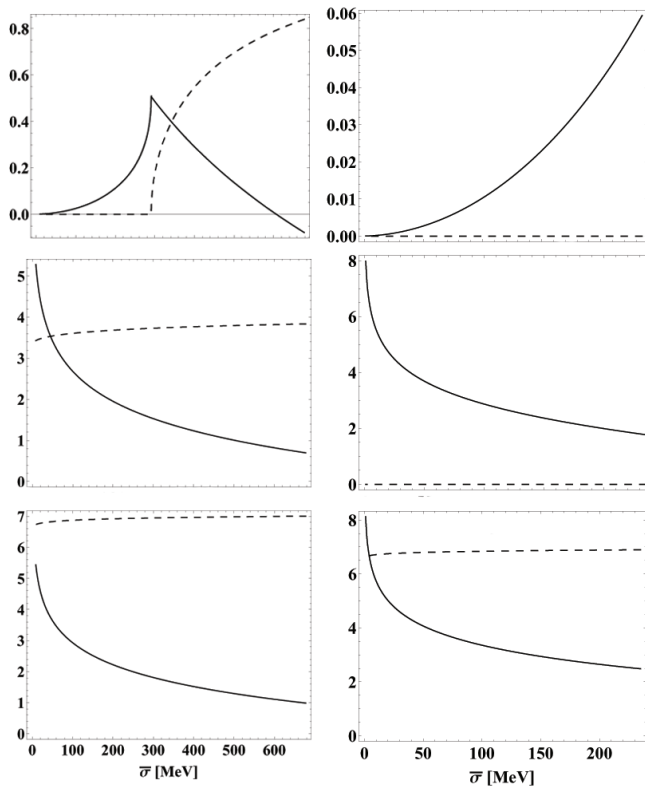


FIG. 4. Behavior of the first three poles of the propagator, with a Gaussian regulator, as a function of $\bar{\sigma}$ for set A (plots on the left) and set B (plots on the right). The solid lines represent $\text{Re}(q^2/\Lambda^2)$ and the dashed lines represent $\text{Im}(q^2/\Lambda^2)$

As can be seen from Fig. 5, for set A, $\bar{\sigma}$ rises with temperature between $T \approx 80 - 110$ MeV. This is exactly the kind of thermal instability found in [26]. However, for set B there is no such instability. Let us recall that the main difference between sets A and B was the presence of a pole with a negative real part in set A. One could suspect then that the rising of $\bar{\sigma}$ with temperature in set A is a consequence of the presence of this odd pole. To better understand this, let us solve again Eq. (28) but now for three different cases: considering the first three poles of set A, considering only the first pole of set A and considering only the second and third poles of set A.

As can be seen from Fig. 6 when we take into account the first pole (solid and dashed lines in Fig. 6) the instability remains. When we consider only the second and third poles (dotted line in Fig. 6), the initial rising is gone, but a new rising appears now at a higher temperature. However, this is not totally unexpected. The second and third poles of the propagator have imaginary parts of the same order of their real parts, meaning they are particles whose decay widths are of the same order than their masses. Such a quasiparticle is a highly

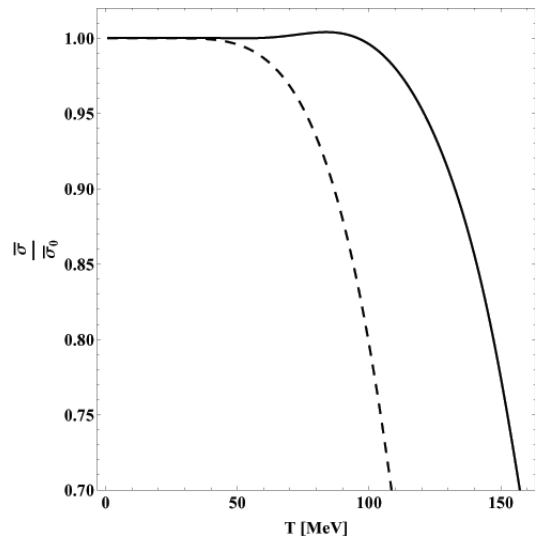


FIG. 5. Behavior of $\bar{\sigma}$ as a function of temperature. The solid line corresponds to set A and the dashed line to set B. In both cases the the first three poles of the propagator are being considered.

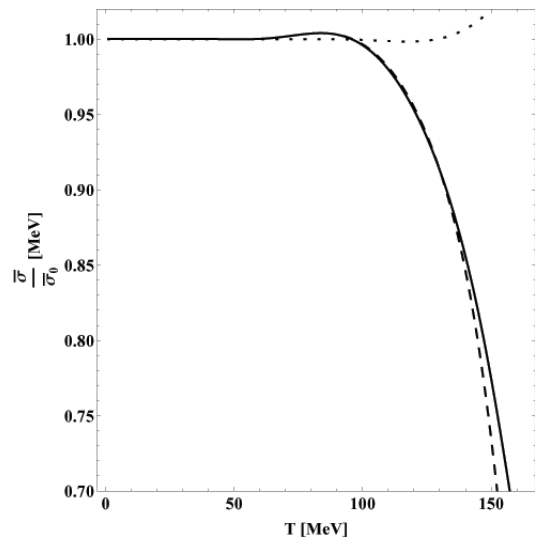


FIG. 6. Behavior of $\bar{\sigma}$ as a function of temperature. The solid line corresponds to the solution for the first three poles of set A. The dashed is the solution with only the first pole of set A and the dotted line is the solution with only the second and third poles of set A.

unstable one and one should expect some odd behavior when considering its condensation. Furthermore, since we have a decay width of the same order of the mass, it is not clear that this can be interpreted as a quasiparticle since it corresponds to a very wide resonance.

This analysis has been performed with the Gaussian regulator because it allows to compare the results of this

article to those of reference [26], however, the Gaussian regulator is far from ideal to study these situations. On the one hand it has an infinite number of poles which makes the full computation extremely challenging. On the other hand the pole with a negative real part is also the only pole that, at lower $\bar{\sigma}$, is a stable pole with a vanishing imaginary part. This means that the same pole that, presumably, produces the instability is the only “well behaved” pole that will also make our condensate rapidly decrease as temperature increases. In this manner it seems that achieving the usual behavior for $\bar{\sigma}$ when considering the Gaussian regulator with parameter set A may be impossible. Because of this, it is useful to consider other regulators, such as the Lorentzian regulator, that exhibit a finite number of poles and thus allows us to better study how each pole affects the behavior of $\bar{\sigma}$.

IV. INTEGER LORENTZIAN REGULATOR.

Let us now consider the following regulator in Minkowski space

$$r(q^2) = \frac{1}{1 + \left(-\frac{q^2}{\Lambda^2}\right)^2}. \quad (32)$$

The following parameters are taken from [37]: $m = 4.6$ MeV, $\bar{\sigma}_0 = 216$ MeV, $\Lambda = 868$ MeV and $G\Lambda^2 = 9.61$. Eqs. (30) and (31) can be solved to find the poles of the propagator with this regulator

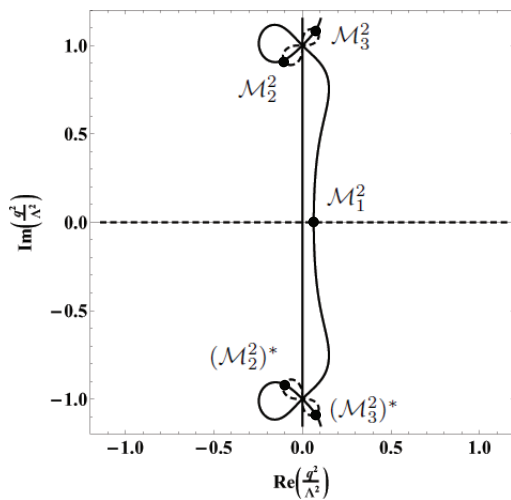


FIG. 7. Poles of the propagator for the integer Lorentzian regulator. The dashed lines are solutions to Eq. (31) and the solid lines solutions to Eq. (30)

As can be seen from Fig. 7 there are three poles for this regulator. One of the poles is real (\mathcal{M}_1) while the other two are complex conjugate pairs, and one of them (\mathcal{M}_2) has a negative real part. Similarly to what was

done in the previous section Eq. (28) can be solved to get the behaviour of $\bar{\sigma}$ as a function of temperature. It will be done in three different cases: By counting all of the three poles, by counting only \mathcal{M}_1 and by counting only \mathcal{M}_2 .

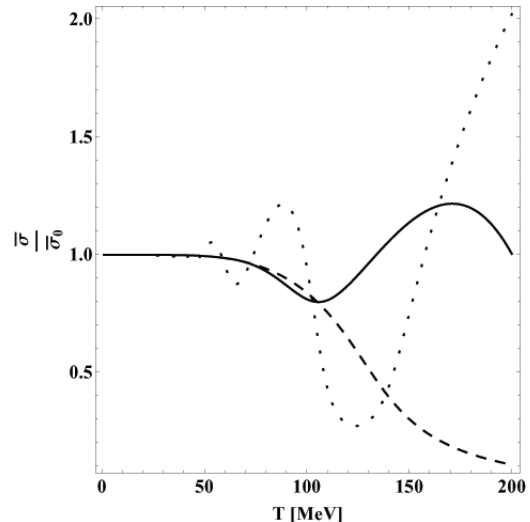


FIG. 8. Behavior of $\bar{\sigma}$ as a function of temperature. The solid line corresponds is solution from counting all the poles. The dashed line is the solution for counting only \mathcal{M}_1 and the dotted line is the solution for counting only \mathcal{M}_2 .

As can be seen from Fig. 8 instabilities appear with this regulator as well. However, if we only consider the real pole (the dashed line in Fig. 8) then we have no instability. The instability seems to arise from the pole with a negative real part. If we only consider this pole (dotted line in Fig. 8) then the instabilities become much larger. This is the same type of behavior that was present with the Gaussian regulators. Those quasiparticles that are tachyons seem to produce these type of thermal instabilities. However, if they are neglected, then the instabilities seem to disappear. It is important to note that, even though tachyons seem to cause bigger instabilities, quasiparticles with decay widths of the same order (or bigger) than their mass also produce instabilities. As was already mentioned, the physical interpretation of this states as well defined particles is not clear, and so, the appearance if instabilities is to be expected. However, this instabilities should be smaller than those produced from negative squared mass states. To illustrate this, we can plot the behavior of $\bar{\sigma}$ by considering now only \mathcal{M}_1 and \mathcal{M}_3 .

As can be seen from Fig. 9 even though the pole with the negative real part has been neglected (dashed line in Fig. 9) we still have an instability. This is due to the fact that we are still considering a very unstable quasiparticle, that is, we are considering a pole with a positive real part, but a much bigger imaginary part. This states are still expected to yield some instability and it is not clear that they can be described as quasiparticles. Just as in

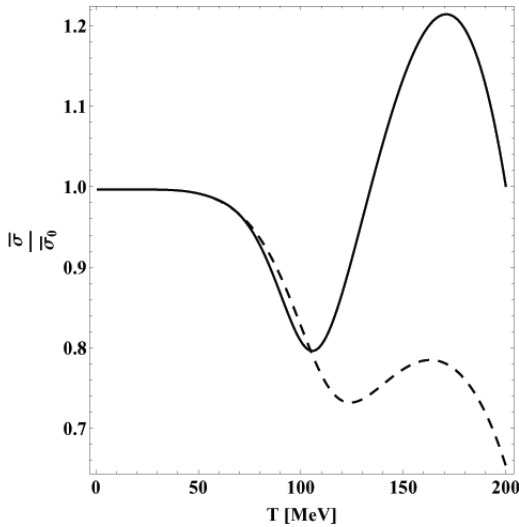


FIG. 9. Behavior of $\bar{\sigma}$ as a function of temperature. The solid line corresponds is solution from counting all the poles. The dashed line is the solution for counting only \mathcal{M}_1 and \mathcal{M}_3 .

the Gaussian case, it is the real pole that one is sure that produces no instability. One might expect the same thing from a complex pole with a small imaginary part, i.e. a well defined quasiparticle. However, none of the regulators considered so far exhibits such a pole. This will be the case in the next section.

V. FRACTIONAL LORENTZIAN REGULATOR.

Lorentzian regulators with fractional exponents have become interesting because they are able to reproduce lattice data from the light quark propagator [28]. Inspired by that we consider the following regulator in Euclidean space

$$r(q_E^2) = \frac{1}{1 + \left(\frac{q_E^2}{\Lambda^2}\right)^{3/2}}. \quad (33)$$

On performing the rotation to Minkowski space one has to define how the half integer exponent will be understood [1]. In Minkowski space, momentum may take complex values and so the regulator is a multivalued function of the momentum. If we take $q^2/\Lambda^2 \equiv Re^{i\theta}$, then we define in Minkowski space

$$r(q^2) = \frac{1}{1 + R^{3/2}e^{\frac{3}{2}i(\theta+\pi)}}. \quad (34)$$

With this definition the multivalued nature of our regulator is preserved. Therefore there will be two Riemann sheets and hence, poles for our propagator will be found in both sheets. This propagator will then have several poles. For our analysis we will work in the chiral limit

where $m = 0$. In this manner the number of poles is significantly reduced and the model is better suited to study the effects of each pole as is the aim of this article. The following parameters are taken from [1]: $m = 0$ MeV, $\bar{\sigma}_0 = 261$ MeV, $\Lambda = 635$ MeV and $G\Lambda^2 = 10.81$.

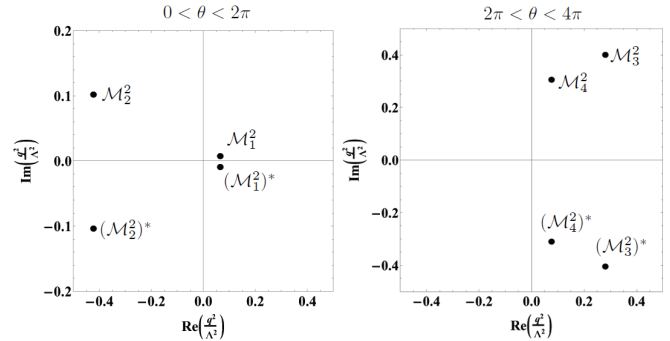


FIG. 10. Poles of the propagator for the half-integer Lorentzian regulator.

In Fig. 10 the poles of the propagator are shown. There is one pole with a negative real part in the first sheet (\mathcal{M}_2). In the second sheet there are two other poles with big imaginary parts (\mathcal{M}_3 and \mathcal{M}_4). So far, one would expect some instabilities from the poles in the second sheet and also from \mathcal{M}_2 in the first sheet. However, in the first sheet, we also have one pole with a positive real part and a small imaginary part (\mathcal{M}_1). This is exactly the kind of pole that was not present neither in the Gaussian regulator nor in the integer Lorentzian regulator and one would expect a stable behavior from such pole.

As can be seen from Fig. 11 an instability is present when all of the poles of the model are considered. If only the first pole (\mathcal{M}_1 in Fig. 10) is taken into account, then the instability disappears. However, if we take into account only the second pole (\mathcal{M}_2 in Fig. 10), which is the one with the negative real part, then we can see the same instability we see when we count all of the poles. This reinforces the statement that such instabilities arise from considering condensates of highly unstable quasiparticles. If we were to consider the behavior of $\bar{\sigma}$ by counting only \mathcal{M}_1 , \mathcal{M}_3 and \mathcal{M}_4 , then the solution would just overlap with the dashed line in Fig. 10. This is because \mathcal{M}_3 and \mathcal{M}_4 are much more massive than \mathcal{M}_1 , and hence, the latter dominates the behavior of $\bar{\sigma}$.

VI. HANDLING THE INSTABILITIES.

So far, it has been shown in agreement with [26], that thermal instabilities arise in nNJL models. It was argued that these instabilities are a consequence of the presence of tachyonic modes, i.e. quasiparticle states

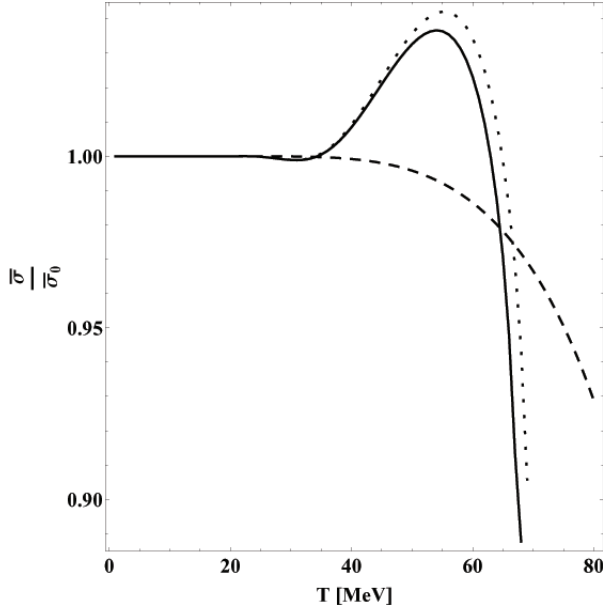


FIG. 11. Behavior of $\bar{\sigma}$ as a function of temperature. The solid line corresponds to solution from counting all the poles. The dashed line is the solution from counting only \mathcal{M}_1 and the dotted line is the solution from counting only \mathcal{M}_2 .

with negative squared masses, and states whose decay width is of the same order, or bigger, than their mass. There are a few ways in which these instabilities may be handled. On the one hand, one could treat these states as unphysical and so, exclude them from the analysis. This can formally be done by slightly deforming the integration path in Fig. 1 around these unphysical poles so that they will not contribute to the SDF and hence, they will not appear in our propagator. Also, one could simply ask for the model to not exhibit such poles and look for a parameter set where all of the poles are well defined quasiparticles with real masses and decay widths smaller than these masses.

In [26] it has been shown that the inclusion of the Polyakov loop in the model also contributes to soften these instabilities. In the next section it will be analyzed how the Polyakov loop affects the poles of the propagator. Particularly, how it affects the poles with negative squared mass and, based on this analysis, why it contributes to soften the instabilities.

VII. THE POLYAKOV LOOP AND SOFTENED INSTABILITIES.

The Polyakov loop $\langle \Phi \rangle$ is defined as [25]

$$\langle \Phi(\mathbf{x}) \rangle = \frac{1}{N_c} \langle \text{tr}_c [L(\mathbf{x})] \rangle, \quad (35)$$

where tr_c is a trace over color indices and

$$L(\mathbf{x}) = \mathcal{P} \exp \left[i \int_0^\beta d\tau A_4(\tau, \mathbf{x}) \right]. \quad (36)$$

Here, \mathcal{P} is the path-ordering operator and A_4 is the fourth component, in Euclidean space, of the gluon fields. The Polyakov loop can be incorporated into the model through the substitution $p_\mu \rightarrow p_\mu + A_\mu$ [25]. The Polyakov gauge [41] is considered, where only A_μ^3 and A_μ^8 are nonvanishing and, as in [42–46], $A_\mu^8 = 0$. Then, in Minkowski space

$$A_\mu = i \frac{\lambda_3}{2} A_0^3 \delta_{\mu 0} \equiv i \frac{\lambda_3}{2} \phi \delta_{\mu 0}, \quad (37)$$

where λ_3 is the third Gell-Mann matrix in $SU(3)$ color space. The propagator is then

$$S(p) = (\not{p} - \Sigma(p))^{-1} \quad (38)$$

where $p_0 = q_0 + \frac{i\phi}{2}\lambda_3$ and $\mathbf{p} = \mathbf{q}$, q being the four-momentum in Minkowski space. To look at the poles of the propagator, it can be rewritten like

$$S(p) = (\not{p} + \Sigma(p))(\not{p} + \Sigma(q))^{-1}(\not{p} - \Sigma(q))^{-1}. \quad (39)$$

Here $(\not{p} + \Sigma(q))^{-1}(\not{p} - \Sigma(q))^{-1}$ is a matrix in Lorentz and color space. This matrix can be inverted and the propagator rewritten as

$$S(\phi, q) = \frac{\not{p} + \Sigma}{(q^2 - \Sigma^2(q))[(q^2 - \Sigma^2(q) - \phi^2/4)^2 + q_0^2 \phi^2]} \mathbf{K}, \quad (40)$$

where $\mathbf{K} = \mathbf{I} \otimes \mathbf{L}$. Here, \mathbf{I} is the identity matrix in Lorentz space and \mathbf{L} is a matrix in color space with no singularities

$$\mathbf{L} = \text{diag} \left((q^2 - \Sigma^2(q)) \left(q^2 - \Sigma^2(q) - i q_0 \phi - \frac{\phi^2}{4} \right), \right. \\ \left. (q^2 - \Sigma^2(q)) \left(q^2 - \Sigma^2(q) + i q_0 \phi - \frac{\phi^2}{4} \right), \right. \\ \left. \left| q^2 - \Sigma^2(q) + i q_0 \phi - \frac{\phi^2}{4} \right|^2 \right) \quad (41)$$

From Eq. (40) it is clear that the usual poles we had at $q^2 - \Sigma^2(q) = 0$ are still there, but new poles have been added through the Polyakov loop. Such poles are solutions to

$$(q^2 - \Sigma^2 - \phi^2/4)^2 + q_0^2 \phi^2 = (q^2 - \Sigma^2(q) - \phi^2/4)^2 \\ + (q^\mu A_\mu^3)^2 = 0. \quad (42)$$

This last equation is explicitly Lorentz covariant, so poles can be searched for in a reference frame where $\mathbf{q} = 0$. In this manner, the new poles that have been

included through the Polyakov loop can be found by solving $(q_0^2 - \Sigma^2 - \phi^2/4)^2 + q_0^2 \phi^2 = 0$. Of course, for $\phi = 0$ we recover the poles we had before. This allows to study the behavior of a single pole as a function of the Polyakov loop. Let us look at the pole with a negative real part that arose whenset of parameters A for the Gaussian regulator was studied.

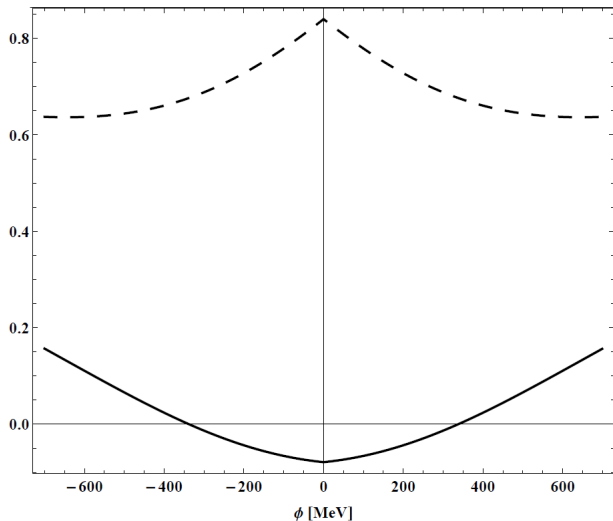


FIG. 12. Behavior of the negative real part pole from set A of the Gaussian regulator as a function of the Polyakov loop. The solid line is the real part of the pole and the dashed line is the imaginary part. Computation were made at $\bar{\sigma} = \bar{\sigma}_0$

Figure 12 shows the evolution of the pole with a negative real part as a function of the Polyakov loop. As can be seen, the real part of the pole becomes positive at large enough ϕ . Not only this, but also the imaginary part becomes smaller. This means that this pole will behave better in presence of a Polyakov loop. This explains why the thermal instabilities are softened by the Polyakov loop. It includes new poles that are better behaved than the ones we had before and so, it is to expect that the thermal instabilities should be reduced.

VIII. CONCLUSIONS.

The appearance of thermodynamic instabilities in the thermal nonlocal NJL model for three different regulators has been studied. It was found that the appearance of instabilities is closely related to the presence of unstable quasiparticles in the model. Specifically, poles of the propagator with negative squared masses seem to produce big instabilities and poles with decay widths of the same order, or bigger, than the mass also produce instabilities. On the other hand, positive real poles and poles with small imaginary parts, seem to exhibit the usual behaviour one would expect from a condensate.

These instabilities can be removed by neglecting unphysical poles, i.e. tachyons and poles with big decay widths. In order to do so, one can deform the integration path when computing the SDF and so exclude these poles from the propagator. One can also choose a different set of parameters that do not exhibit these unphysical poles. In both of these cases, instabilities will not arise and one should observe the usual behavior that is expected from a condensate.

It has also been shown that the Polyakov loop softens these instabilities. It is found that including the Polyakov loop in the model means to include additional poles that are less unstable than the poles previously considered. Furthermore, as can be seen from Fig. 12, for high enough values of the Polyakov loop, tachyonic modes may turn into well defined quasiparticles with positive squared masses. This means then that the instabilities will be softened because of the higher stability of the poles.

IX. ACKNOWLEDGEMENTS.

The author would like to thank M. Loewe and C. Villavicencio for helpful discussion. The author would like to acknowledge support from FONDECYT under gran No. 1130056 and CONICYT under Grant No. 21110577.

-
- [1] M. Loewe, F. Marquez, and C. Villavicencio, Phys.Rev. D **88**, 056004 (2013).
 - [2] M. De Francia, H. Falomir, and M. Loewe, Phys.Rev. D **55**, 2477 (1997).
 - [3] M. De Francia, H. Falomir, and M. Loewe, Phys.Rev. C **60**, 055203 (1999).
 - [4] E. Fraga, L. Palhares, and C. Villavicencio, Phys.Rev. D **79**, 014021 (2009).
 - [5] C. D. Roberts and A. G. Williams, Prog.Part.Nucl.Phys. **33**, 477 (1994).
 - [6] C. D. Roberts and S. M. Schmidt, Prog.Part.Nucl.Phys. **45**, S1 (2000).
 - [7] D. Blaschke, G. Bureau, Y. Kalinovsky, P. Maris, and P. Tandy, Int.J.Mod.Phys. A **16**, 2267 (2001).
 - [8] C. E. Detar and T. Kunihiro, Phys.Rev. D **39**, 2805 (1989).

- [9] R. Delbourgo and M. Scadron, *Mod.Phys.Lett. A* **10**, 251 (1995).
- [10] J. T. Lenaghan, D. H. Rischke, and J. Schaffner-Bielich, *Phys.Rev. D* **62**, 085008 (2000).
- [11] M. Loewe, C. Villavicencio, and R. Zamora, *Phys. Rev. D* **89**, 016004 (2014).
- [12] Y. Nambu and G. Jona-Lasinio, *Phys.Rev.* **122**, 345 (1961).
- [13] Y. Nambu and G. Jona-Lasinio, *Phys.Rev.* **124**, 246 (1961).
- [14] M. Loewe, A. Jorge Ruiz, and J. Rojas, *Phys.Rev. D* **78**, 096007 (2008).
- [15] A. Radzhabov, D. Blaschke, M. Buballa, and M. Volkov, *Phys.Rev. D* **83**, 116004 (2011).
- [16] D. Blaschke, P. Costa, and Y. Kalinovsky, *Phys.Rev. D* **85**, 034005 (2012).
- [17] M. Buballa, *Phys.Rept.* **407**, 205 (2005).
- [18] S. Klevansky, *Rev.Mod.Phys.* **64**, 649 (1992).
- [19] R. Bowler and M. Birse, *Nucl.Phys. A* **582**, 655 (1995).
- [20] R. S. Plant and M. C. Birse, *Nucl.Phys. A* **628**, 607 (1998).
- [21] M. Loewe, P. Morales, and C. Villavicencio, *Phys.Rev. D* **83**, 096005 (2011).
- [22] V. Pagura, D. Gomez Dumm, and N. Scoccola, *Phys.Rev. D* **87**, 014027 (2013).
- [23] D. Gomez Dumm and N. N. Scoccola, *Phys.Rev. D* **65**, 074021 (2002).
- [24] G. Contrera, M. Orsaria, and N. Scoccola, *Phys.Rev. D* **82**, 054026 (2010).
- [25] T. Hell, S. Roessner, M. Cristoforetti, and W. Weise, *Phys.Rev. D* **79**, 014022 (2009).
- [26] S. Benic, D. Blaschke, and M. Buballa, *Phys.Rev. D* **86**, 074002 (2012).
- [27] S. Benic, D. Blaschke, G. Contrera, and D. Horvatic, (2013).
- [28] S. Noguera and N. Scoccola, *Phys.Rev. D* **78**, 114002 (2008).
- [29] J. I. Kapusta, *Finite-temperature field theory* (Cambridge University Press, 1993).
- [30] I. Ojima, *Annals Phys.* **137**, 1 (1981).
- [31] H. Matsumoto, I. Ojima, and H. Umezawa, *Annals Phys.* **152**, 348 (1984).
- [32] R. Kobes, G. Semenoff, and N. Weiss, *Z.Phys. C* **29**, 371 (1985).
- [33] N. Landsman and C. van Weert, *Phys.Rept.* **145**, 141 (1987).
- [34] M. Le Bellac, *Thermal field theory* (Cambridge University Press, 2000).
- [35] A. Das, *Finite temperature field theory*, Vol. 16 (World Scientific Singapore, 1997).
- [36] L. Dolan and R. Jackiw, *Phys.Rev. D* **9**, 3320 (1974).
- [37] D. Gomez Dumm, A. Grunfeld, and N. Scoccola, *Phys.Rev. D* **74**, 054026 (2006).
- [38] G. N. Felder, L. Kofman, and A. D. Linde, *Phys.Rev. D* **64**, 123517 (2001).
- [39] G. Feinberg, *Phys.Rev.* **159**, 1089 (1967).
- [40] G. Feinberg, *Phys. Rev. D* **17**, 1651 (1978).
- [41] A. M. Polyakov, *Phys.Lett. B* **72**, 477 (1978).
- [42] S. Roessner, C. Ratti, and W. Weise, *Phys.Rev. D* **75**, 034007 (2007).
- [43] S. Roessner, T. Hell, C. Ratti, and W. Weise, *Nucl.Phys. A* **814**, 118 (2008).
- [44] D. Gomez Dumm, D. Blaschke, A. Grunfeld, and N. Scoccola, *Phys.Rev. D* **78**, 114021 (2008).
- [45] H. Abuki, M. Ciminale, R. Gatto, N. Ippolito, G. Nardulli, *et al.*, *Phys.Rev. D* **78**, 014002 (2008).
- [46] H. Abuki, M. Ciminale, R. Gatto, G. Nardulli, and M. Ruggieri, *Phys.Rev. D* **77**, 074018 (2008).